Optimal Architecture Design of Dual-Mode Hybrid-electric Powertrain

Alparslan Emrah Bayrak, Yi Ren, and Panos Papalambros

Abstract

Hybrid-electric vehicle architectures have been commercialized to serve different categories of vehicles and driving conditions. Such architectures can be optimally controlled by switching among driving modes, namely, the power distribution schemes in their planetary gear (PG) transmissions, in order to operate the vehicle in the most efficient regions of engine and motor maps. We propose a systematic way to identify the optimal architecture for a given vehicle drive cycle, rather than parametrically optimizing one or more pre-selected architectures. To this end, we develop an automatic generator of feasible driving modes for a given number of PGs. In an illustrative study, 1724 unique modes are generated for a powertrain consisting of one engine, two motors and one or two PGs. We then search for a near-optimal dual-mode architecture for the given drive cycle and vehicle specification, and we demonstrate how changes in vehicle weight and driving cycle affect the optimal architecture.

Index Terms

Power-split hybrid vehicle, optimal configuration design, bond graph.

I. Introduction

A variety of hybrid-electric vehicle (HEV) architectures have been commercialized to date. For a given architecture, one or more "driving modes" of the planetary gear (PG) transmission determine the distribution of power among engine, motors and output shaft. Optimal fuel efficiency and drivability can be achieved by controlling mode-shifting, engine, and motor outputs, so that the engine and motors operate in their most efficient regions. For example, the Chevrolet Volt four-mode architecture with one engine, two motors and one PG can switch among modes to gain fuel efficiency in different driving conditions such as launching (low-speed high-torque) and highway (high-speed low-torque) drives.

All authors are with the Department of Mechanical Engineering, University of Michigan, Ann Arbor.

Existing HEV architectures include one-PG [8], [15], two-PG [11], [10], [4], [3], [2] and even three-PG [13], [9] systems. The optimal architecture may change based on given vehicle weight and drive cycle. For example, the fuel efficient architecture of a military combat vehicle may vary from that of a city-driving truck [6], [7]. Searching for an optimal powertrain architecture is a challenging problem: The number of feasible driving modes grows quickly as the number of components, e.g., engines, motors and planetary gears, increases. The illustrative study in this paper shows that there are more than one thousand unique driving modes for two-PG systems and over five thousands for three-PG ones. Furthermore, an optimal architecture may consist of multiple driving modes, leading to the combinatorial problem of mode choices for the architecture. In previous work, Zhang et al. examined a set of clutching options based on the Toyota Prius architecture with one PG [15]; Liu and Peng found the optimal single-mode architecture for a two-PG system by filtering some 288 power-split modes [7]. While these approaches are effective, the general design automation problem of generating and optimizing a multi-mode powertrain architecture for a given number of elements, vehicle specifications and driving cycle, is yet to be addressed.

This paper describes such a design automation process. We introduce a bond graph representation of driving modes and propose a mode generation algorithm that enumerates all feasible HEV and EV modes, given a set of powertrain components. We then use a heuristic search algorithm to identify the best architecture, i.e., the combination of modes that optimizes fuel consumption for a given drive cycle. The performance of each architecture is tested in simulation, with an optimal control algorithm called Equivalent Consumption Minimization Strategy (ECMS) incorporated to achieve balanced battery State of Charge (SOC).

In the remainder of the paper, we introduce the bond graph representation in Section II, assuming basic familiarity with bond graph terminology. Section III describes the algorithm for automatic driving mode generation. Section IV discusses the vehicle component models used for simulation and the settings of the ECMS algorithm. Section V describes the optimal design process in a case study. We conclude and discuss future directions in Section VI.

II. HEV Modes as Bond Graphs

In this section, we define a driving mode and show that each mode can be represented by a bond graph. Consider the Toyota Prius powertrain system with four power sources: Engine,

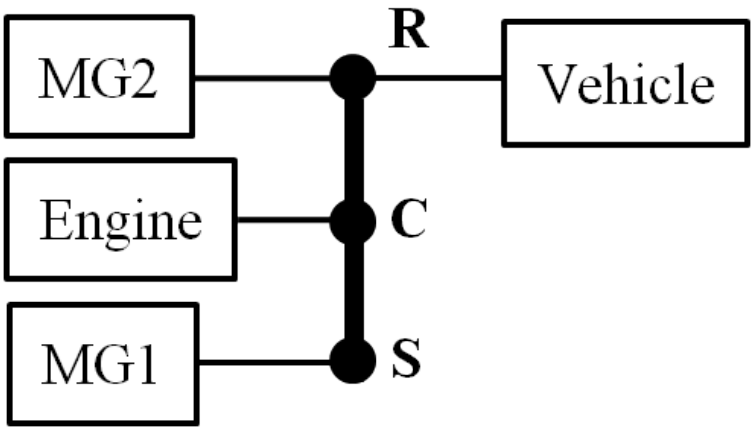

Fig. 1. The Toyota Prius Hybrid System in the lever analogy representation; four powertrain components (the engine, two motors and the vehicle output shaft) are connected to PG nodes.

vehicle and two motor/generators are shown in Figure 1. These four sources are connected together by means of a planetary gear (PG), shown as the lever in the figure, with nodes "R" for the ring, "C" for the carrier and "S" for the sun gear. We use $\omega_{1,2,3,4}$ and $T_{1,2,3,4}$ to represent the speed (rads/s) and torques (Nm) that go out from the PG to the engine, the vehicle, Motor 1 and Motor 2, respectively. We assume engine and motor inertias are negligible compared to the vehicle shaft. Therefore $\omega_{1,3,4}$ and $T_{1,3,4}$ are equivalently the engine and motor speeds and torques, while ω_2 and T_2 are the speed and torque demands from the vehicle, rated by the final drive ratio. For a certain PG ratio ρ, the speed relationship of the system is given by

$$\begin{aligned} (\rho+1)\omega_1 &= \omega_3 + \rho\omega_2, \\ \omega_4 &= \omega_2; \end{aligned} \tag{1}$$

and the static torque relationship is given by

$$\begin{aligned} -T_1 &= T_3(1+\rho), \\ T_1\rho + T_4(1+\rho) &= T_2(1+\rho). \end{aligned} \tag{2}$$

From Equations (1) and (2), the engine speed and torque are decoupled from the vehicle speed and torque demands. This is made possible by operating Motor 1 at a certain speed so that the combined speed of Motor 1 and the engine output from the PG will meet the speed demand. Meanwhile, the output torque from the PG is combined with Motor 2 torque to meet the torque

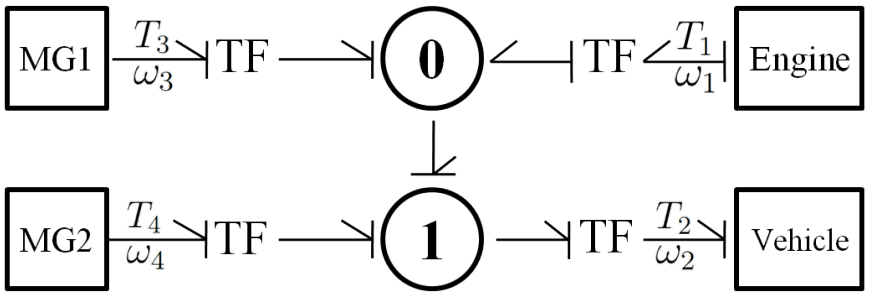

Fig. 2. The bond graph of the Prius System.

demand. Therefore the required power is split and met by two sources. This power-split design allows the engine to run at its own efficient region (in the speed - torque map) and thus improve fuel economy. We call Equations (1) and (2) the state-space output equations of a driving mode of the Prius single-mode architecture.

We now introduce bond graphs as a more general representation of driving modes. To illustrate, Figure 2 presents the Prius bond graph. We use square boxes for external sources and circles with 0 and 1 for "0" and "1" junctions. The sign "TF" represents a transformer that scales torque and speed simultaneously by a transformer modulus for constant power before going into "0" or "1" junctions. For the Prius mode, the "0" junction sends the combined flows from the engine and Motor 1 to the vehicle, while the "1" junction combines the torque from Motor 2 and that from the "0" junction. The scale factors on the transformers follow the gear ratio of the PG. For brevity, in the rest of this paper we will remove the transformer blocks on bonds and treat transformer modulus as bond weights.

The bond graph representation allows us to create different modes by changing the graph structure. Sample bond graph representations of existing driving modes are shown in Figure 3. Notice from this figure that some architectures, such as the Alison Hybrid System (AHS) [12] and the Ai and Anderson architecture [2], contain multiple modes, and mode switching is enabled through clutches. For example, in AHS Mode 1, the clutch between PG2 and ground is engaged, resulting in higher output torque at vehicle launch; when the vehicle reaches a high speed, the two PGs are connected through a second clutch, leading to a more fuel efficient high speed mode.

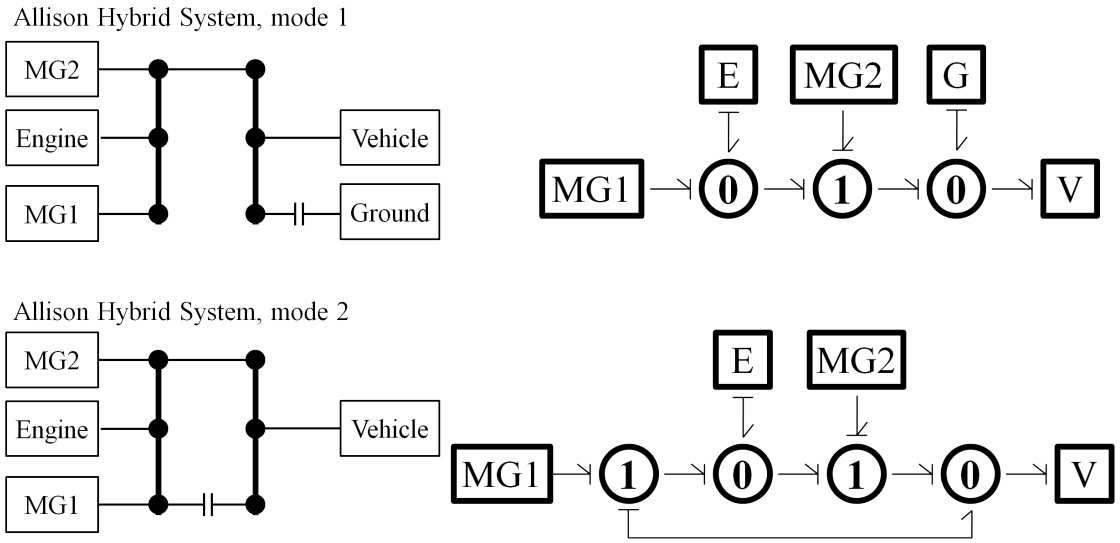

(a) Allison Hybrid System (AHS) [12]

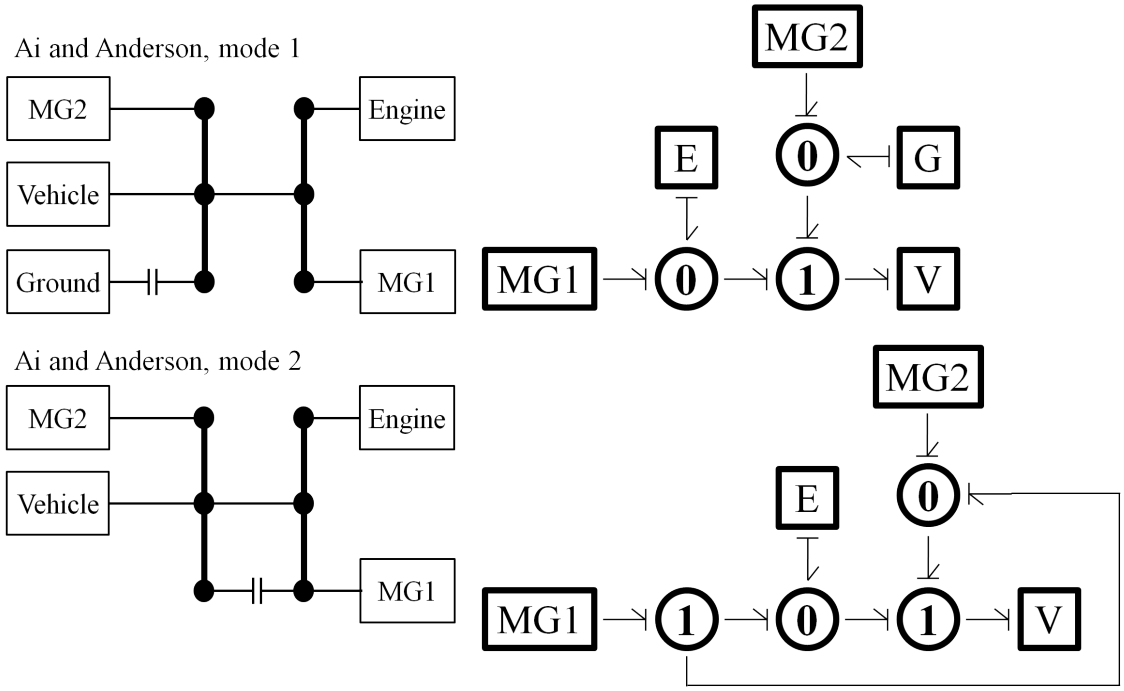

(b) Ai and Anderson [2]

Fig. 3. Bond graphs of modes in existing architectures. “E” stands for engine, “V” for vehicle output shaft, “G” for ground and “MG1” and “MG2” for the two motor/generators.

III. Mode Generation

We now describe how we can generate all feasible modes for a given set of powertrain components. We will call power sources the "external" junctions, and "0" and "1" junctions the "internal" ones. The number of internal junctions will depend on the number of PGs we use and whether a PG node is grounded. More details are given later in this section.

In the following, we elaborate on the four steps of mode generation: (i) All possible undirected graphs are enumerated for a given number of PGs; (ii) for each graph, internal junctions are labeled as either "0" or "1" and causality strokes are assigned to bonds; (iii) bond weights are assigned, determining how powertrain components are connected to PG nodes; (iv) the resulting bond graphs are then processed to generate the corresponding state space output equations.

A. Graph enumeration

We discuss the enumeration procedure for all undirected graphs with J^{ext} external junctions and J internal ones. To do so, some bond graph properties shall be introduced first.

To begin, a valid bond graph must be simple and connected: A simple graph has no more than one bond between any two junctions and does not contain loops on a single junction, see Figure 4; a connected graph is defined here as such that any two junctions are connected (by a graph path) regardless of bond directions. Each external junction must have exactly one bond connecting to an internal junction, representing the input (or output) torque and speed flow from (or to) this external junction. We show below that for any junction with more than three bonds, there exists an equivalent graph containing internal junctions with only three bonds. Therefore in the rest of the paper we assume that an internal junction has exactly three bonds.

Bond Graph Property 1. *A junction with n bonds can be replaced by a series of $n-2$ junctions with three bonds each.*

Proof. Without loss of generality, we use "1" junction in this proof. In Figure 5, the bond graph on the left establishes the following torque (ω) and speed (T) relationships:

$$\begin{aligned} T_1 + T_2 - T_3 - T_4 = 0; \\ \omega_1 = \omega_2 = \omega_3 = \omega_4. \end{aligned} \tag{3}$$

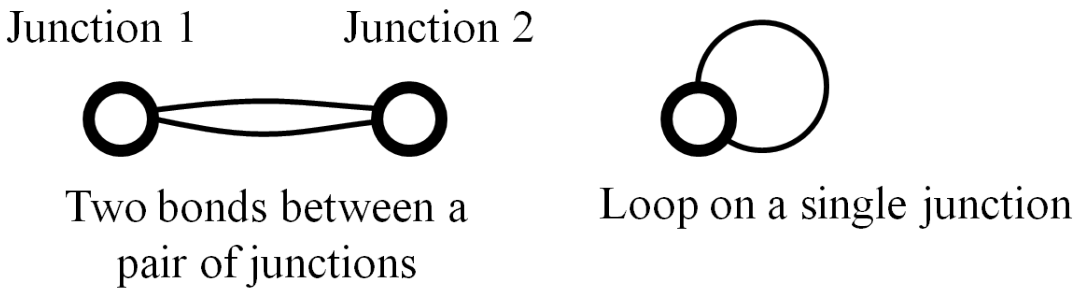

Fig. 4. A simple graph has no more than one bond between any two different junctions and does not contain loops on single junctions.

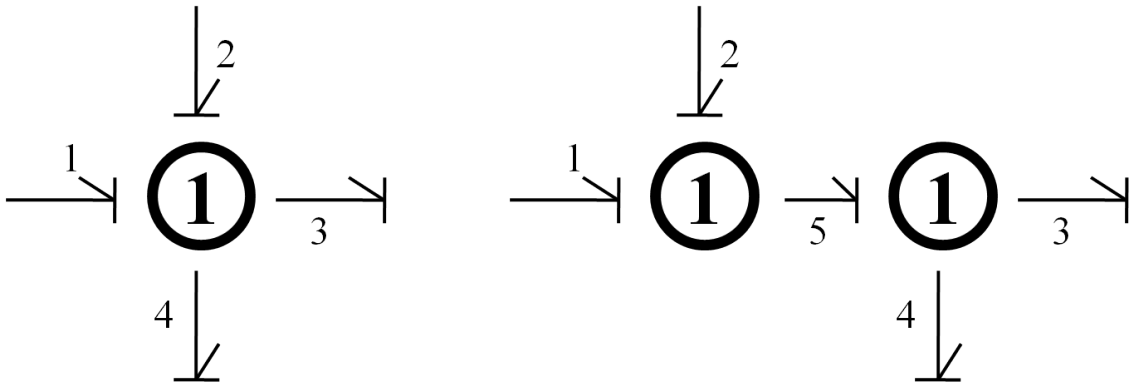

Fig. 5. A bond graph with more than three bonds (left) and its equivalent counterpart with exactly three bonds (right).

These are equivalent to the relationships imposed by the bond graph on the right, for which we have:

$$\begin{aligned} T_1 + T_2 - T_5 &= 0; \\ T_5 - T_3 - T_4 &= 0; \\ \omega_1 = \omega_2 = \omega_3 = \omega_4 &= \omega_5. \end{aligned} \tag{4}$$

More generally, one can replace a "1" junction with n bonds with a "1" junction with $n-1$ bonds connected to another "1" junction with three bonds. We can then show that, if the property holds for a junction with $n-1$ bonds, it also holds for a junction with n bonds. Therefore, the property can be proved by induction. The same proof holds for a "0" junction. □

The second property says that a bond graph must have an even number of junctions, i.e., an odd number of external junctions must yield an odd number of internal ones and vice versa.

Bond Graph Property 2. *A bond graph must have an even number of junctions if each internal junction has three bonds and each external one has one bond.*

Proof. Following Property 1, a bond graph will have $(3J - J^{\text{ext}})/2 + J^{\text{ext}}$ number of bonds. Therefore $3J - J^{\text{ext}}$ must be even, and so as $J + J^{\text{ext}}$. □

The external junctions considered here include the vehicle, the engine, two motors and optionally, the ground. When the ground is not engaged, the graph has four external junctions and requires two or four internal junctions, representing a mode with one PG or two PGs, respectively; when one of the PG nodes is engaged to the ground, five external junctions exist and three internal junctions are required to accomodate all powertrain components for one or two-PG systems. The mode generation method can be extended to systems with an arbitrary number of PGs. Here, we limit the number of junctions for two reasons: (1) The computational cost of mode generation increases quickly with the number of internal junctions, and (2) a driving mode involving many PGs will likely have little practical value.

We now show how graphs with a given number of external and internal junctions are enumerated. The adjacency matrix of a graph can be denoted as $\mathbf{G} = [\mathbf{0}\ \mathbf{A}; \mathbf{A}^T\ \mathbf{B}]$, where $\mathbf{A}$ $(J^{\text{ext}} \times J)$ and $\mathbf{B}$ $(J \times J)$ are binary matrices. Element $A_{ij} = 1$ ($B_{ij} = 1$) if and only if the ith external (internal) junction and the jth internal junction are connected. Thus, by definition, $\mathbf{B}$ is symmetric. Also, external junctions are not connected with each other, hence the zero block in the adjacency matrix. A realization of $\mathbf{A}$ and $\mathbf{B}$ will determine a graph when the following constraints are satisfied:

1) Each external junction has one bond:

$$\sum_{j=1}^{J} A_{ij} = 1, \quad \forall i = 1, 2, ..., J^{\text{ext}}. \tag{5}$$

2) Each internal junction has three bonds:

$$\sum_{j=1}^{J^{ext}} A_{ji} + \sum_{j'=1}^{J} B_{ij'} = 3, \quad \forall i = 1, 2, ..., J. \tag{6}$$

The enumeration procedure can be summarized by two steps: All feasible $\mathbf{A}$s are first generated; based on each $\mathbf{A}$, $\mathbf{B}$s can be created to satisfy Equation (6).

Replicated modes (graphs) with different ordering of internal junctions can be created by this procedure, see Figure 6. We consider graph $\mathcal{G}_1$ a replicate of graph $\mathcal{G}_2$ when the matrix $\mathbf{G}_1$ can

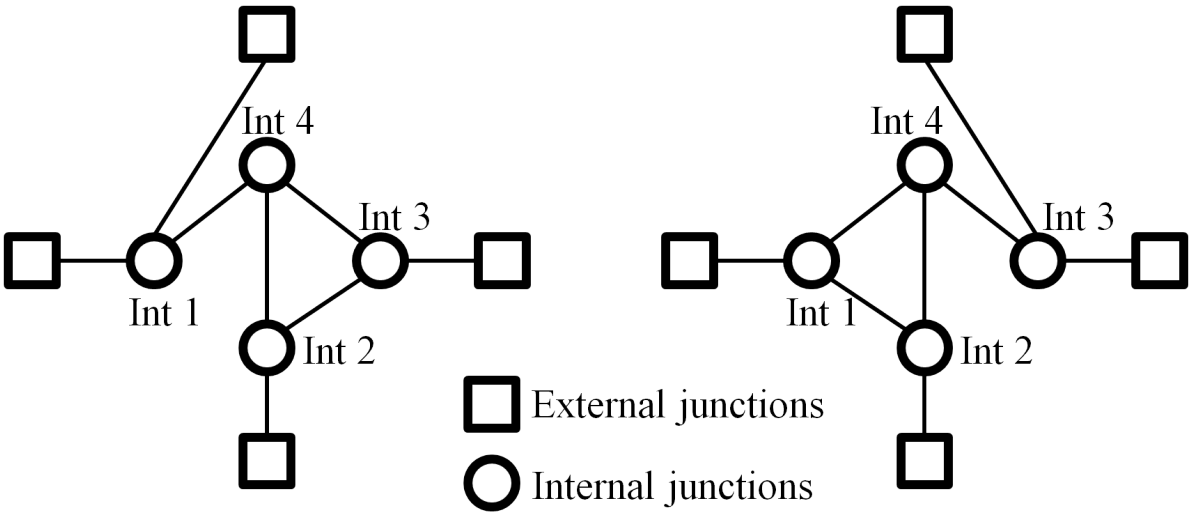

Fig. 6. An example of replicates with different ordering of internal junctions. After assigning junction types and bond weights, these two graphs will generate multiple identical state space output equations. Therefore, one graph should be removed before proceeding to the next step.

be transformed into $\mathbf{G}_2$ by reordering its rows and columns simultaneously, i.e., $\exists \mathbf{P},\ \mathbf{P}^T\mathbf{P} = \mathbf{I},\ \mathbf{P}^T\mathbf{G}_1\mathbf{P} = \mathbf{G}_2$. Since replicates will have the same eigenvalues as the original graph, we can easily filter them out by this criterion.

Throughout the discussion below we will use $\mathcal{V}$ ($|\mathcal{V}| = J$) and $\mathcal{E}$ ($|\mathcal{E}| = (3J - J^{\text{ext}})/2$) for the internal junction and bond sets, respectively. The ith element in $\mathcal{V}$ ($\mathcal{E}$) is denoted as $\mathcal{V}_i$ ($\mathcal{E}_i$). We use the mapping $e(j_1, j_2) = \mathcal{E}_j$ to return the jth bond in $\mathcal{E}$ connecting junctions j_1 and j_2. For simple graphs, the mapping $e(j_1, j_2)$ returns a unique index when the junctions j_1 and j_2 are adjacent, i.e., $G_{j_1 j_2} = 1$.

B. Junction type assignment

The next step is to assign junction types and causal strokes to bonds. We will show that, similar to graph enumeration, the procedure can be summarized as finding feasible binary solutions for a system of linear equations. With the same convention as in Section II, we use external junctions 1 through 5 to represent the engine, the vehicle output shaft, Motor 1, Motor 2 and the ground, respectively. The engine and the vehicle are usually defined as the flow (speed) sources while the motors as the effort (torque) ones. The ground is a special flow source where the flow is always zero. Notice that some exceptions exist in pure EV modes. For example, when the engine

is connected to the ground directly, it becomes a torque source as its flow is fixed to zero by the ground; or when the engine is excluded from the system, one of the motors must substitute the engine and become a flow source.

Consider an internal junction j with junction type t_j. We define $t_j = 1$ when the junction type is "1" and $t_j = -1$ when it is "0". We assign $c_{j_1 j_2} = 1$ to the bond connecting junctions j_1 and j_2 when the causal stroke of this bond is at junction j_1, implying $c_{j_2 j_1} = -1$. A valid bond graph requires that among the three bonds of a "1" ("0") junction, two (one) of them should have the casual stroke at this junction. Based on the bond graph causality requirement, we should have the following equality constraint on internal junction j_1:

$$-t_{j_1} + \sum_{j_2 : G_{j_1 j_2} = 1} c_{j_1 j_2} = 0, \quad \forall j_1 = 1, 2, .., J. \tag{7}$$

Since the number of binary variables in Equation (7) is $|\mathcal{V}|+|\mathcal{E}|$ while the number of equations to be satisfied is $|\mathcal{V}|$, multiple solutions exist. Notice that the solutions to Equation (7) have the following property:

Bond Graph Property 3. *When the engine and vehicle are flow sources and the two motors are effort sources, the numbers of "0" and "1" junctions are equal when J is even, while the number of "0" junctions is one more than that of "1" junctions when J is odd.*

The proof is given below where we denote by J_0 and J_1 the numbers of "0" and "1" junctions, respectively, satisfying $J_0 + J_1 = J$.

Proof. Let J be even. From Equation (7) we have:

$$\sum_{j_1=1}^{J} \left(-t_{j_1} + \sum_{j_2 : G_{j_1 j_2} = 1} c_{j_1 j_2} \right) = 0. \tag{8}$$

Notice that the causality strokes on bonds associated with external junctions are given and their stroke values sum up to zero since two of them are effort sources and the other two are flow sources. Further, in Equation (8), for each $c_{j_1 j_2}$ and for all j_1 and j_2, there exists $c_{j_2 j_1}$ such that $c_{j_1 j_2} + c_{j_2 j_1} = 0$. Therefore by summing up all equations from Equation (8) we get:

$$\sum_{j_1=1}^{J} t_{j_1} = 0, \tag{9}$$

which requires $J_0 = J_1$ for an even J. The same proof applies when J is odd, with the stroke value on the bond associated with the ground being -1 (a flow source), in which case the right hand side of Equation (9) becomes -1. □

This property implies that given engine and vehicle as flow sources and motors as effort ones, a graph with $J = 2k$ nodes will model a k-PG mode and a graph with $J = 2k + 1$ nodes will model a $(k + 1)$-PG mode where one PG node is engaged to the ground. Similarly, we can also show that when the engine is directly connected to the ground and thus becomes an effort source, a graph with $J = 2k + 1$ nodes will model a k-PG pure EV mode.

C. Bond weight assignment

From the examples in Section II, a pair of "0" and "1" junctions in a bond graph can be realized by a planetary gear where the gear ratio ρ is determined by the weights on the associated bonds. Here we assume a fixed ratio $\rho = 2$ for all planetary gear sets. Figure 7 shows all six combinations of bond weights for a "0" junction, where each combination has different assignments of the sun, ring and carrier nodes to the associated bonds. For example, the top-left combination uses node "1" as the sun, node "2" as the carrier and node "3" as the ring. For a given graph, we first enumerate all combinations of bond weights on its "0" junctions. We then look for shared bonds between any two "0" junctions. These shared bonds could have two different weights assigned from the previous step, representing the connection between two different nodes from two PGs, e.g., the ring node of one PG connected to the carrier of the other. In this situation, the least common multiple will be assigned to the shared bond as its weight and all other bonds of the two "0" junctions will be updated accordingly. An example of this procedure is shown in Figure 8.

D. State space output equation generation

With a bond graph created, we can generate its state space output equations. Define the vector $\boldsymbol{\omega}^{\text{ext}} = [\omega_1, \omega_2, \omega_3, \omega_4, \omega_5]^T$ with its components being the angular velocities of the engine, the vehicle output shaft to the final drive, the two motors and the ground, respectively. Note that $\omega_5 = 0$ as the ground is always fixed. Define also the vector of angular velocities on internal bonds as $\boldsymbol{\omega}$. Then we have the system of linear equations:

$$\mathbf{W}_0\boldsymbol{\omega}^{\text{ext}} + \mathbf{W}\boldsymbol{\omega} = \mathbf{0}, \tag{10}$$

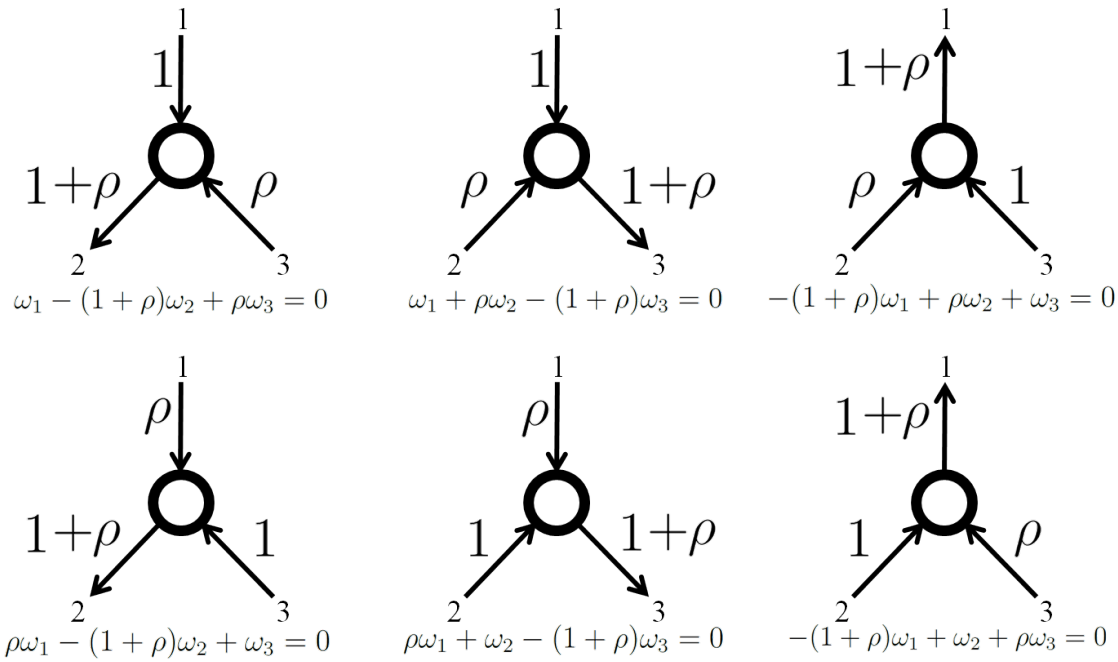

Fig. 7. Six possible combinations for one "0" junction, switching roles of sun, ring and carrier of the three associated bonds.

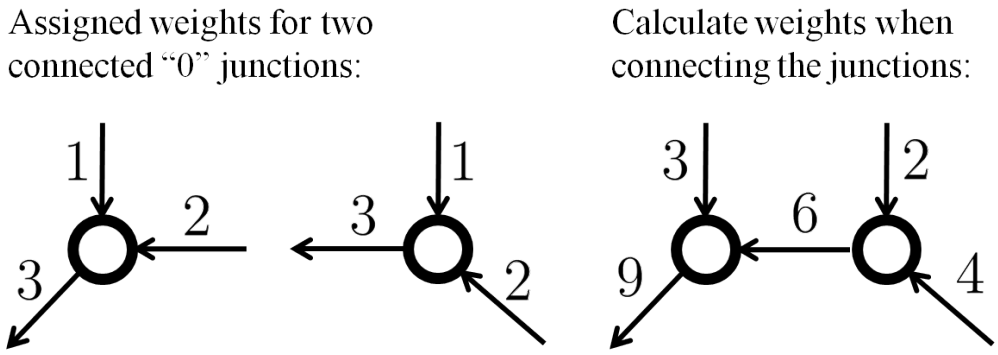

Fig. 8. When two "0" junctions share one bond, the actual bond weights must be adjusted based on the assigned values.

where $[\mathbf{W}_0, \mathbf{W}]$ can be calculated using bond weights and velocity relationships at "0" and "1" junctions. The matrix $\mathbf{W}$ has $J_0 + 2J_1$ rows since each "0" junction has one equality constraint and each "1" junction has two. It also has $|\mathcal{E}|$ columns according to the length of $\boldsymbol{\omega}$. Using bond graph Property 3, it is easy to verify that $J_0 + 2J_1 > (3J - J^{\text{ext}})/2$ when $J^{\text{ext}} > 1$. Therefore $\mathbf{W}$

has more rows than columns. When $\mathbf{W}$ has full column rank, Equation (10) can be rewritten as:

$$(\mathbf{W}_0 - \mathbf{W}(\mathbf{W}^T\mathbf{W})^{-1}\mathbf{W}^T\mathbf{W}_0)\omega^{\text{ext}} = \mathbf{0}. \tag{11}$$

We can further decompose $(\mathbf{W}_0 - \mathbf{W}(\mathbf{W}^T\mathbf{W})^{-1}\mathbf{W}^T\mathbf{W}_0)$ as $[\bar{\mathbf{W}}_1, \bar{\mathbf{W}}_2]$ where both $\bar{\mathbf{W}}_1$ and $\bar{\mathbf{W}}_2$ are four-by-two matrices. When both $\bar{\mathbf{W}}_2^T\bar{\mathbf{W}}_1$ and $\bar{\mathbf{W}}_2^T\bar{\mathbf{W}}_2$ are invertible (and taking $\omega_5 = 0$ into account when the ground is considered), Equation (11) can be further rewritten as:

$$[\omega_3, \omega_4]^T = (\bar{\mathbf{W}}_2^T\bar{\mathbf{W}}_2)^{-1}\bar{\mathbf{W}}_2^T\bar{\mathbf{W}}_1[\omega_1, \omega_2]^T. \tag{12}$$

Equation (12) determines the flow relationship in two-DOF systems. When the gear energy losses and engine and motor inertias are negligible, energy conservation requires that the power input from engine and motors equals the power output to the vehicle:

$$\omega_1 T_1 + \omega_3 T_3 + \omega_4 T_4 = \omega_2 T_2. \tag{13}$$

Denoting $\mathbf{C} = (\bar{\mathbf{W}}_2^T\bar{\mathbf{W}}_2)^{-1}\bar{\mathbf{W}}_2^T\bar{\mathbf{W}}_1$, Equations (12) and (13) lead to

$$[\omega_1, \omega_2]\left(\mathbf{C}^T[T_3, T_4]^T - [-T_1, T_2]^T\right) = 0. \tag{14}$$

Since Equation (14) holds for any arbitrary ω_1 and ω_2, we have

$$[T_3, T_4] = [-T_1, T_2]\mathbf{C}^{-1}. \tag{15}$$

Equations (12) and (15) are used to calculate motor speeds (torques) based on engine and vehicle speeds (torques), when the system has two DOFs. From our enumeration, all valid hybrid modes are two-DOF while some pure EV modes can have one DOF, such as in Figure 10(a). The state space equations for a one DOF system without the engine will be as follows with constants $c_{2,3,4}$ derived from Equations (11) and (13). When one of the motor speeds is free to vary, we have:

$$\begin{aligned} c_2\omega_2 + c_3\omega_3 + c_4\omega_4 &= 0 \\ T_3 &= -\frac{c_3}{c_2}T_2 \\ T_4 &= -\frac{c_4}{c_2}T_2, \end{aligned} \tag{16}$$

or when one of the motor torques is free to vary, we have:

$$\begin{aligned} c_2T_2 + c_3T_3 + c_4T_4 &= 0 \\ \omega_3 &= -\frac{c_3}{c_2}\omega_2 \\ \omega_4 &= -\frac{c_4}{c_2}\omega_2. \end{aligned} \tag{17}$$

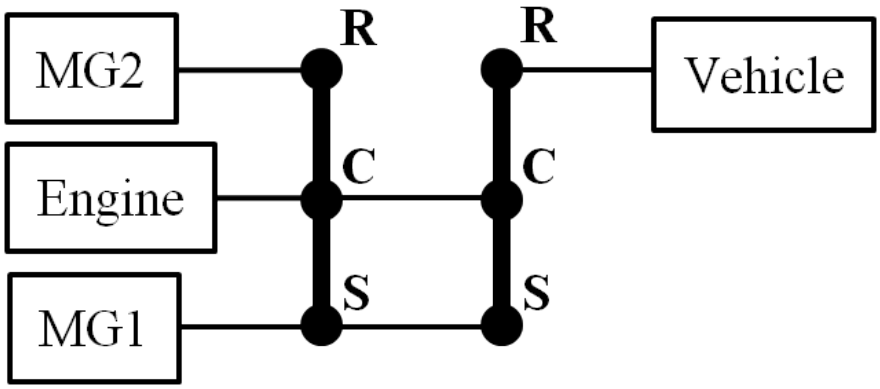

(a) Toyota Prius-like 2-PG mode

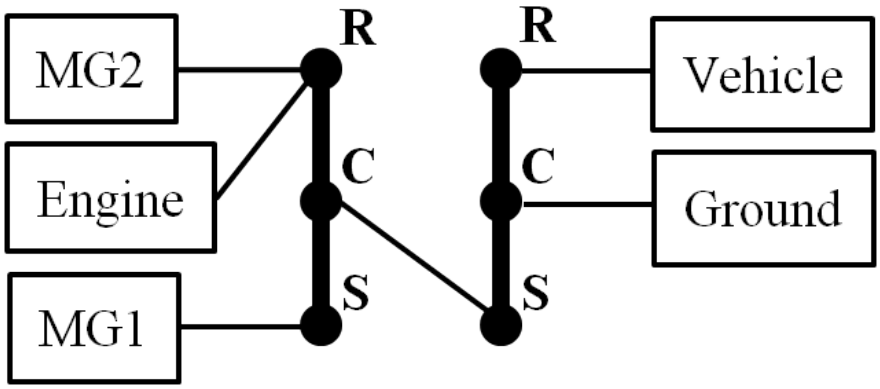

(b) Chevrolet Volt-like 2-PG mode, the PG on right serves as an extra final drive.

Fig. 9. 2-PG modes similar to Toyota Prius in (a) and Chevrolet Volt in (b).

E. Results for 2-PG mode architecture

Following the mode generation procedure above, we generate in total 1724 unique modes. Among them, 1116 hybrid modes are generated, incorporating the engine, two motors and two PGs, with and without a "ground" node. All feasible two-PG modes are found, including existing ones such as those in [2], [12], [5]. Notably, we also found the two-PG counterparts of Toyota Prius and the dual-motor mode of Chevrolet Volt, as shown in Figure 9.

Among all EV modes, there are 559 modes where the engine and the ground are connected together at one PG node, see Figures 10(a) and 10(b) for examples; and another 49 modes where the engine and ground are excluded, see Figure 10(c) for an example.

The number of modes derived here is more than that from [7], which only considers two-PG

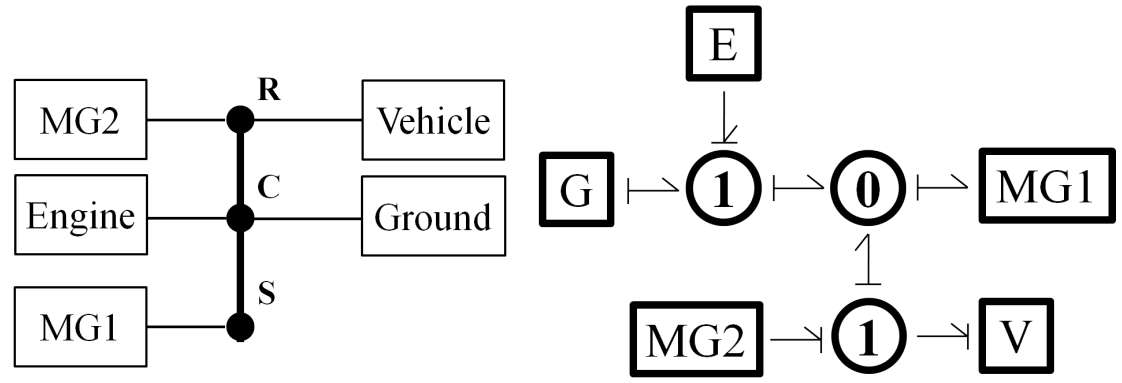

(a) one-PG EV mode, engine engaged to the ground

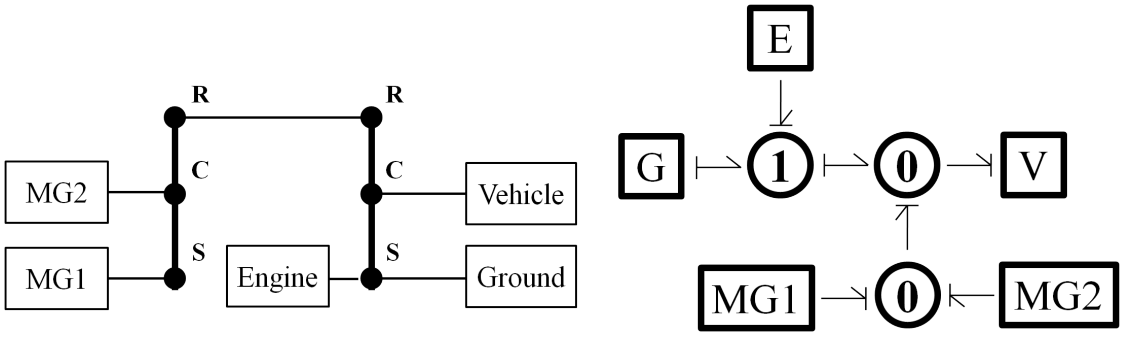

(b) two-PG EV mode, engine engaged to the ground

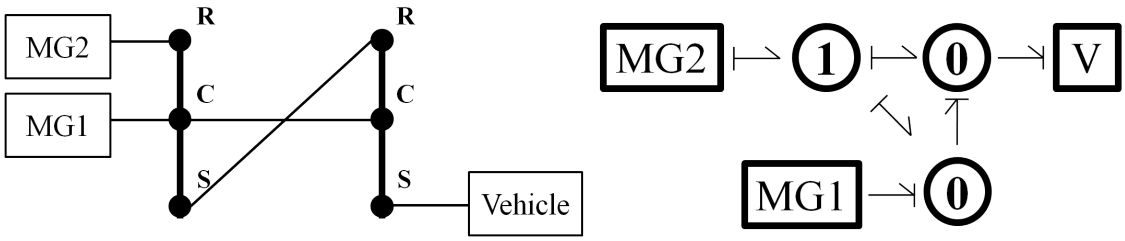

(c) EV mode without engine

Fig. 10. Examples of EV modes

modes and does not allow two power sources to be connected to one PG node. The proposed method does not consider multiple grounded PG nodes or negative PG ratios used in a Ravigneaux compound planetary gear set. Nonetheless, these can be incorporated when such alternatives are of interest.

TABLE I

VEHICLE SPECIFICATIONS

Specification	**Value**
Vehicle Body Mass	1400 [kg]
Tyre Radius	0.3 [m]
Frontal Area	2 [m^2]
Aerodynamic Drag Coefficient	0.29
Battery Voltage	350 [V]
Battery Nominal Capacity	6.5 [Ah]
Battery Efficiency	92%
Invertor Efficiency	95%
Electric Motor Output Power	50 [kW] (rated)
Engine Output Power	43 [kW] (1.5 [L])

IV. VEHICLE MODEL AND CONTROL

A set of modes generated from the previous section form an architecture which is then exported to a vehicle model. The performance of an architecture is defined by its optimal fuel efficiency on a certain drive cycle. This efficiency is obtained using the Equivalent Consumption Minimization Strategy (ECMS) that finds the optimal control policy for engine and motor operations and mode shifting through the drive cycle. This section gives modeling details of the vehicle and describes our implementation of the ECMS algorithm.

A. Vehicle model

The generated modes are incorporated in a vehicle model for performance simulation. We simulate a mid-size passenger car with a high voltage battery, two interior permanent magnet synchronous motor/generators, an engine, a transmission and a vehicle body model. Model specifications are given on Table I.

A static battery model is used to calculate battery losses and state of charge (SOC). We

simplify the model by considering the battery output voltage and internal resistance as constants instead of functions of SOC, since the effect of their variation is negligible within the 40% to 80% SOC operation window of interest. A battery maximum charging current limit of 100 A is set to limit the regenerative braking power. Battery transients are also neglected in the model.

Two equivalent motor/generators are used in the model. The efficiency and maximum/minimum torque maps follow those of a 2006 Toyota Prius. These maps are used to calculate the motor loss and the motor current input to the battery model. A fixed inverter efficiency of 95% is integrated in the efficiency map.

The 1.5L engine model uses a fuel consumption map with respect to engine torques and speeds. A maximum engine torque map is also used to limit the output torque of the engine.

The transmission model consists of a 2-PG transmission and a final drive ratio. A set of state space matrices generated from Section III together with a mode shift signal are passed to the transmission model to calculate the torque and speed relationships among the engine, motors and the vehicle shaft based on a quasi-stationary approach where engine and motor inertias are neglected. Mode shifting loss is not modeled in this study. A final drive ratio of 3.9 is used.

B. Optimal control

The ECMS algorithm for the hybrid modes follows the idea from [1]. The two control variables at each time step are the change in SOC ($\Delta\mathrm{SOC}$) and the mode shift signal. The states are current SOC, driving mode, and vehicle output torque and speed demands following the given drive cycle. Recall that the two degree-of-freedom transmission model decouples the engine operation from the vehicle loads. At each time step, for the given vehicle output torque and speed demands, we iterate over a discrete set of feasible engine torque and speed values to find the set of Pareto-optimal battery power and corresponding engine fuel consumption. The Pareto curves and corresponding engine operation points for each time step and each driving mode are pre-calculated so that the optimal fuel consumption and battery power usage can be "looked up" for a given set of states and control variables.

In the case of pure EV modes, the system DOF reduces to one where there is control over either one of the motor speeds or motor torques. For instance, the mode in Figure 10(b) has one independent motor speed variable while the mode in Figure 10(a) has one independent steady state motor torque variable to be controlled. Therefore, the iteration is performed over

the independent variable in EV modes. In these cases, the Pareto set has only one point as there is no trade-off between battery energy and fuel consumption.

During a drive cycle, the equivalent consumption at each state can be calculated as a sum of instantaneous engine fuel consumption and battery power consumption multiplied by a conversion factor [14]. At a given time step, the optimal control variables are determined by minimizing the equivalent consumption for the given states. We then look up the pre-calculated Pareto curves to find the engine and motor operations corresponding to these control variables. This instantaneous control strategy is proved to be able to calculate the fuel consumption close to the global optimum [14].

Notice that the choice of the conversion factor significantly affects the battery SOC variation over the drive cycle. Therefore, in order to sustain the battery charge at the beginning and end of the drive cycle (at 60% SOC), an appropriate conversion factor needs to be searched for each architecture under evaluation. To this end, we use a simple root-finding algorithm (the secant method) that considers the final SOC as a function of the conversion factor: For a given architecture and drive cycle, the algorithm starts by running two simulations using ECMS with different conversion factors, yielding two final SOC values. A linear function of SOC with respect to the conversion factor is then created and a third conversion factor corresponding to the desired SOC is obtained from this linear interpolation and the true SOC is obtained. The iteration continues with the interpolated conversion factor and another factor that is closest to the desired SOC from previous iterations until a final SOC is obtained within 0.2% error from the target SOC.

V. Optimal Design for a Dual-mode Architecture

In this section, we disucss a tractable search algorithm to find the optimal dual-mode architecture for a given vehicle and drive cycle. We will first apply the algorithm to the base-line vehicle specified in Table I under the UDDS drive cycle. The resulting optimal architecture is compared with an existing fuel-efficient dual-mode design from Zhang et al. [15]. We then show two more architectures optimized for (1) the same vehicle under the HWFET drive cycle and (2) a vehicle with increased weight, in order to investigate how the optimal architecture will vary for different vehicle applications.

A. Search method

The combinatorial problem of finding the optimal architecture involves selecting two modes from 1724 candidates and is computationally expensive[1]. On the other hand, not every combination of modes is feasible. Here we apply the following critical design constraints to reduce the problem size: In any dual-mode architecture, the connection between the vehicle output and a PG node should not contain any cluthes, so that the vehicle can be stably controlled during mode switching. So, any selection of two modes needs to have the vehicle output connected to the same node of the PG set. To comply with this constraint, we collect all modes into three clusters, i.e., "sun", "ring" and "carrier", based on the connection of the vehicle output to the PG. In addition, EV-EV pairing is infeasible due to the charge-sustaining operation constraint at the end of the drive cycle and is not allowed during the search.

Within each cluster, the search starts with an initial mode. The second mode of the architecture is found by enumeration among all other modes in the cluster to minimize the fuel consumption together with the first mode. The algorithm then proceeds to the next iteration where the newly-found mode is now considered as the first mode and a second mode is found in the same way. This simple search algorithm is guaranteed to find new architectures with no more fuel consumption than those from previous iterations. The search continues until the same two modes are selected in two consecutive iterations. The resulting architectures from separate searches within the three mode clusters are then compared and the best one is selected.

B. Results and discussion

The search algorithm is first applied to the vehicle specified in Table I under the UDDS drive cycle. We use the Toyota Prius mode (see Figure 1) as the initial mode for the "ring" cluster. For the "carrier" ("sun") cluster, we start with the Prius mode and switch the connection of the engine (Motor 1) with that of the vehicle output and Motor 2 pair. The search leads to three architectures with 73.2, 73.6 and 69.8 miles per gallon (MPG) from the "ring", "carrier" and "sun" clusters, respectively. The resulting design from the "carrier" cluster, shown in Figure 11, is selected as the optimal architecture.

[1]A single simulation can take 10 to 60 seconds, depending on the convergence of the ECMS conversion factor. Overall the enumeration could take over 2000 days on a desktop with an i7 quad-core CPU.

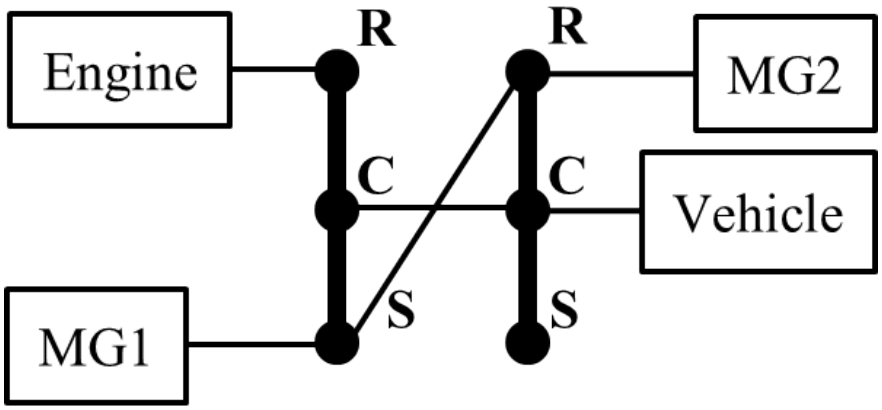

(a) Mode 1 in the optimal architecture

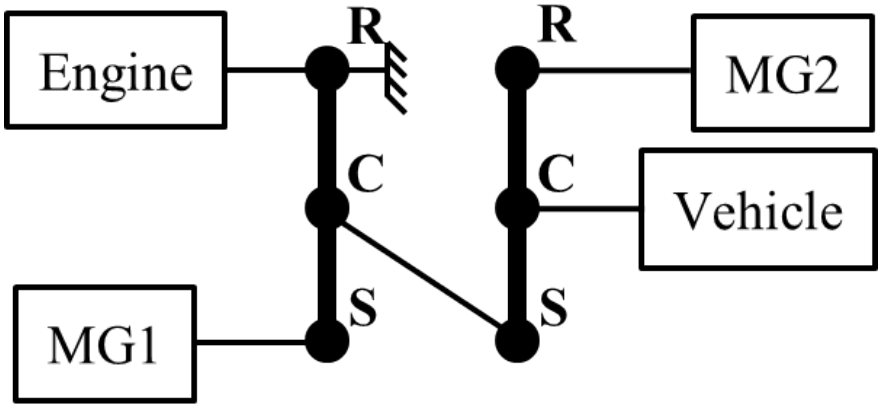

(b) Mode 2 in the optimal architecture

Fig. 11. The optimal solution for 2-mode architecture under UDDS drive cycle

In comparison, the "Prius+" architecture from Zhang et al. [15] has 69.8 MPG for the same vehicle and optimal control settings. Figure 12 compares the fuel consumption curve of the optimal architecture with that of "Prius+", under the UDDS drive cycle. In the same figure, we also show the SOC changes of the two architectures to validate the tuning scheme of the conversion factor. In addition, in order to avoid frequent mode shifting, a penalty of 0.1 gram of equivalent fuel consumption is applied to every mode shift and the resulting mode switching plots are shown for both designs.

To see how the optimal design changes with respect to the drive cycle, we conduct the same optimization using the HWFET drive cycle. This results in 68.7, 67.8, 68.5 MPG for the "ring",

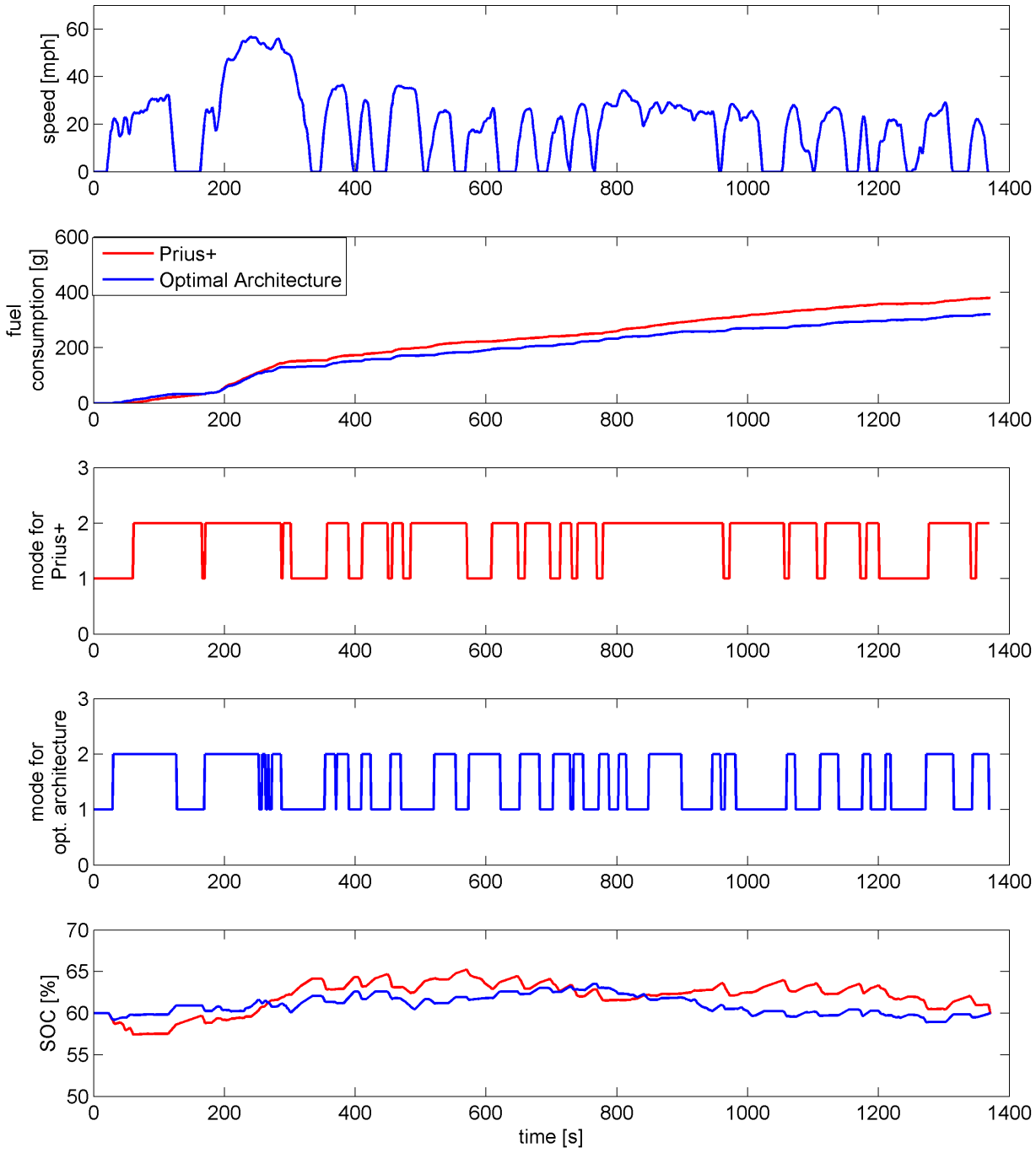

Fig. 12. (From top to bottom) The UDDS drive cycle; Comparison of the fuel consumption of baseline design and the optimal architecture; Change of mode for baseline design; Change of mode for the optimal architecture; Battery SOC variation for the optimal architecture

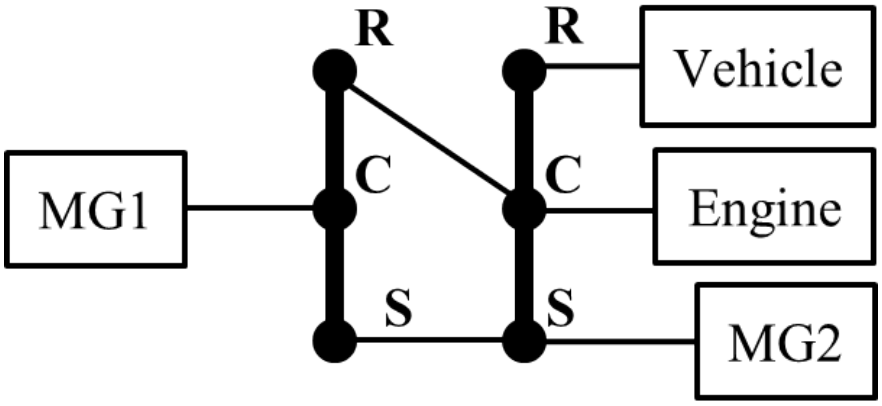

(a) Mode 1 in the optimal architecture

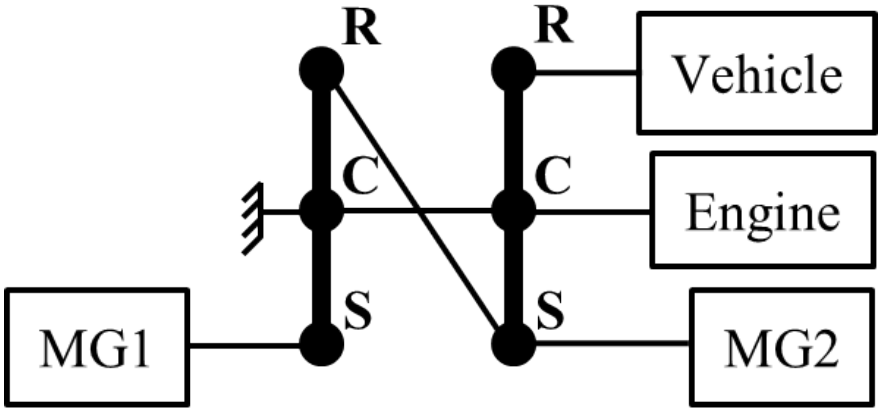

(b) Mode 2 in the optimal architecture

Fig. 13. The optimal solution for 2-mode architecture under HWFET drive cycle starting from the mode on Figure 1

"carrier" and "sun" clusters, respectively. The optimal design from the "ring" cluster is shown in Figure 13. On the other hand, the "Prius+" architecture has 66.8 MPG under HWFET drive cycle. The detailed results for this case are shown in Figure 14. Note that the low shifting frequency in this case is expected since HWFET is a highway cycle and HEV modes are more efficient than EV modes on highway (with high speed and low torque demands).

Finally, we investigate the case where the vehicle mass is increased from 1400 kg to 1600 kg. The optimal architecture comes from the "carrier" cluster with fuel consumption of 68.4 MPG (346.8 grams) and is shown in Figure 15. Note that it has the same HEV mode as the optimal design for the original vehicle but paired with a different EV mode. In fact, the original

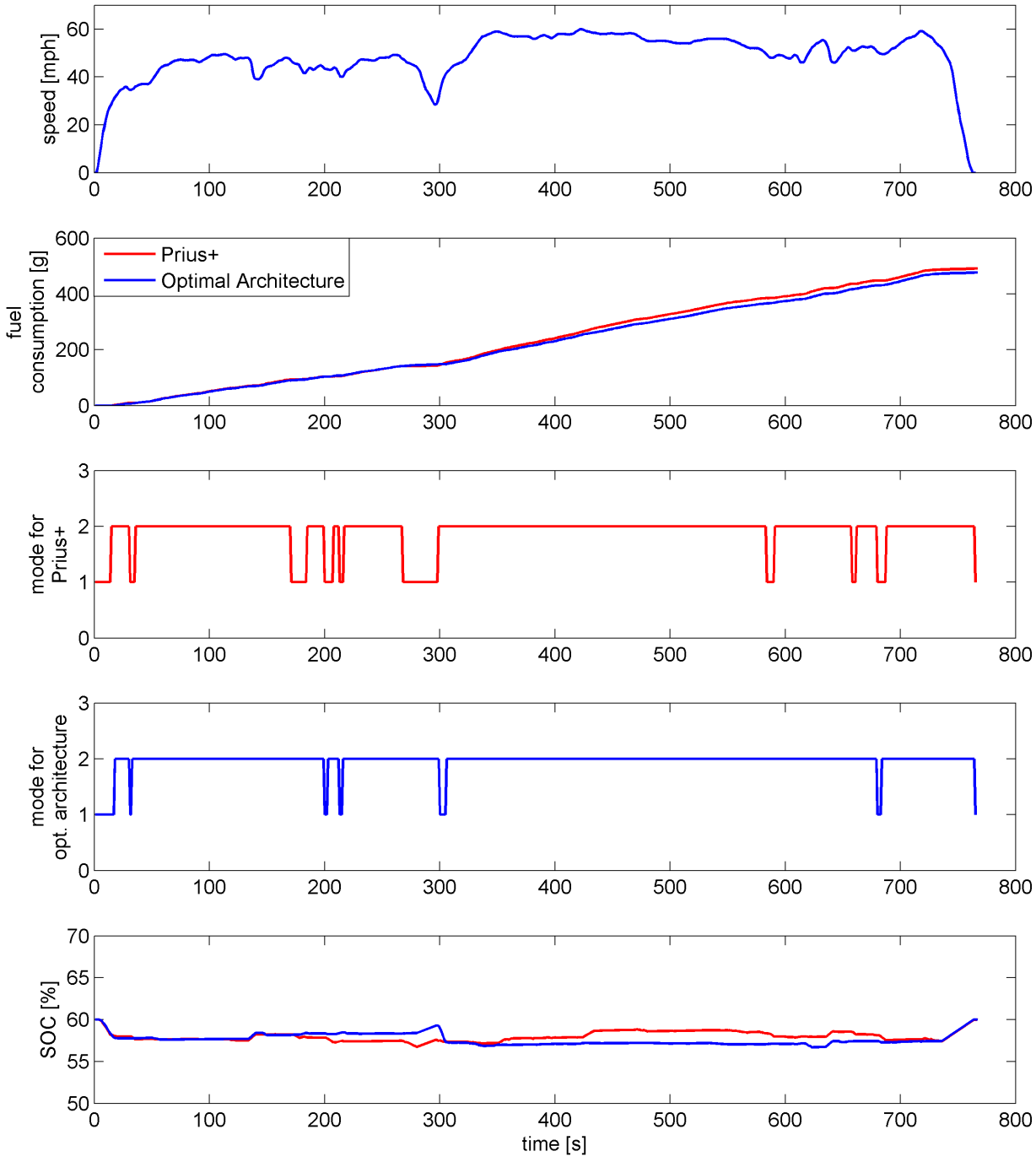

Fig. 14. (From top to bottom) The HWFET drive cycle; Comparison of the fuel consumption of baseline design and the optimal architecture; Change of mode for baseline design; Change of mode for the optimal architecture; Battery SOC variation for the optimal architecture

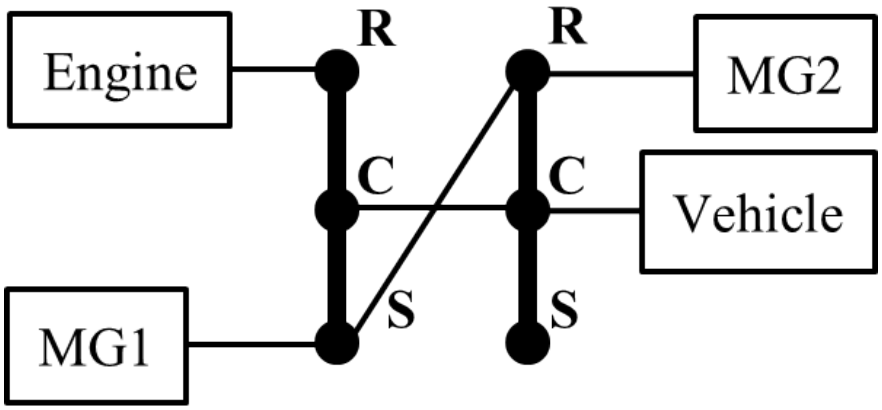

(a) Mode 1 in the optimal architecture

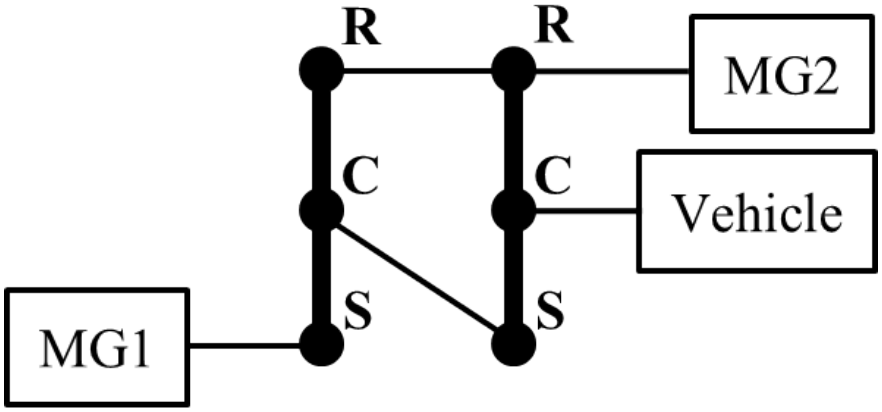

(b) Mode 2 in the optimal architecture

Fig. 15. The optimal solution for 2-mode architecture under UDDS drive cycle for the vehicle with a mass of 1600kg

design in Figure 11 comes very close to the optimal architecture with 68.3 MPG (347.1 grams). This result indicates that the optimal powertrain architecture is sensitive to the change in vehicle weight. Future research should investigate the robustness of architecture design under varying conditions such as vehicle weight.

VI. Conclusions and Future Work

We introduced a systematic way to optimize a dual-model HEV powertrain architecture under given vehicle specifications and drive cycle. The case studies showed that (1) the proposed method can find the optimal architecture with significantly better fuel efficiency than available

designs under the UDDS drive cycle, and (2) the optimal architecture varies depending on the vehicle weight and the chosen drive cycle.

Two modeling issues require future investigation. First, combining modes in an architecture requires a feasibility check. It is possible that a large number of clutches is needed to realize an architecture with the selected modes, making the design unrealistic. To this end, a constraint on the number of clutches might be imposed during optimization. Second, the vehicle weight must be updated based on the architecture when evaluating different possibilities, and packaging feasibility must be checked in order to obtain more realistic results.

While we solely focused on dual-mode two-PG architecture design in this paper, the solution space for exploration can be further expanded by considering multiple modes and planetary gear sets, and variable powertrain parameters such as gear ratios and battery and engine sizes. All of these could also play important roles in further reducing fuel consumption but will also pose challenges to modeling and optimization. The combined design of the architecture and powertrain parameters could lead to intractable computational cost and is yet to be investigated.

VII. Acknowledgement

This research was partially supported by the Automotive Research Center, a US Army Center of Excellence in Modeling and simulation of Ground Vehicle Systems headquartered at the University of Michigan, and by the University of Michigan - General Motors Collaborative Research Laboratory in Advanced Powertrains. This support is gratefully acknowledged. The authors would also like to thank Professor Huei Peng and Xiaowu Zhang from the University of Michigan and Dr. Kukhyun Ahn for their insightful advice. The opinions expressed here are solely those of the authors.

References

[1] K. Ahn, S. Cho, and S. Cha. Optimal operation of the power-split hybrid electric vehicle powertrain. *Proceedings of the Institution of Mechanical Engineers, Part D: Journal of Automobile Engineering*, 222(5):789–800, 2008.

[2] X. Ai and S. Anderson. An electro-mechanical infinitely variable transmisson for hybrid electric vehicles. *SAE Technical Paper 2005-01-0281, doi:10.4271/2005-01-0281*, 2005.

[3] A. Holmes, D. Klemen, and M. Schmidt. Electrically variable transmission with selective input split, compound split, neutral and reverse modes, Mar. 4 2003. US Patent 6,527,658.

[4] A. Holmes and M. Schmidt. Hybrid electric powertrain including a two-mode electrically variable transmission, Nov. 12 2002. US Patent 6,478,705.

[5] N. Kim, J. Kim, and H. Kim. Control strategy for a dual-mode electromechanical, infinitely variable transmission for hybrid electric vehicles. *Proceedings of the Institution of Mechanical Engineers, Part D: Journal of Automobile Engineering*, 222(9):1587–1601, 2008.

[6] C. Li and H. Peng. Optimal configuration design for hydraulic split hybrid vehicles. In *American Control Conference (ACC), 2010*, pages 5812–5817. IEEE, 2010.

[7] J. Liu and H. Peng. A systematic design approach for two planetary gear split hybrid vehicles. *Vehicle System Dynamics*, 48(11):1395–1412, 2010.

[8] J. Liu, H. Peng, and Z. Filipi. Modeling and control analysis of toyota hybrid system. In *IEEE/ASME International Conference on Advanced Intelligent Mechatronics. Proceedings,*, pages 134–139. IEEE, 2005.

[9] M. Raghavan, N. K. Bucknor, and J. D. Hendrickson. Electrically variable transmission having three interconnected planetary gear sets, two clutches and two brakes, Feb. 20 2007. US Patent 7,179,187.

[10] M. Schmidt. Two-mode, input-split, parallel, hybrid transmission, Sept. 24 1996. US Patent 5,558,588.

[11] M. Schmidt. Two-mode, split power, electro-mechanical transmission, Nov. 26 1996. US Patent 5,577,973.

[12] M. Schmidt. Electro-mechanical powertrain, Aug. 10 1999. US Patent 5,935,035.

[13] M. Schmidt. Two-mode, compound-split electro-mechanical vehicular transmission, Aug. 3 1999. US Patent 5,931,757.

[14] L. Serrao, S. Onori, and G. Rizzoni. Ecms as a realization of pontryagin's minimum principle for hev control. In *American Control Conference*, pages 3964–3969. IEEE, 2009.

[15] X. Zhang, C.-T. Li, D. Kum, and H. Peng. Prius+ and volt- : Configuration analysis of power-split hybrid vehicles with a single planetary gear. *IEEE Transactions on Vehicular Technology*, 61(8):3544–3552, 2012.